Hindawi
International Journal of Photoenergy
Volume 2017, Article ID 2562968, 9 pages
https://doi.org/10.1155/2017/2562968

Research Article

A PCBM-Modified TiO_2 Blocking Layer towards Efficient Perovskite Solar Cells

Gang Lu,[1] Fengqin He,[1,2] Shangzheng Pang,[1,2] Haifeng Yang,[2] Dazheng Chen,[2] Jingjing Chang,[2] Zhenhua Lin,[2] Jincheng Zhang,[2] and Chunfu Zhang[2]

[1]*Huanghe Hydropower Solar Industry Technology Co. Ltd., 369 South Yanta Road, Xi'an 710061, China*
[2]*Wide Bandgap Semiconductor Technology Disciplines State Key Laboratory, School of Microelectronics, Xidian University, Xi'an 710071, China*

Correspondence should be addressed to Chunfu Zhang; cfzhang@xidian.edu.cn

Received 17 June 2017; Revised 2 October 2017; Accepted 12 October 2017; Published 7 December 2017

Academic Editor: Giulia Grancini

Organometal halide perovskite as a promising absorber in solar cells has caught tremendous attention in the past few years. Herein, a hydrophobic PCBM layer was introduced into planar heterojunction perovskite solar cells to form the TiO_2/PCBM double blocking layer. The bilayer structure assures the formation of a dense, smooth, and pinhole-free blocking layer. And the PCBM layer can also be in favor of larger grain size perovskite film and further passivate the TiO_2 blocking layer. Scanning electron microscope, atomic force microscope, and X-ray diffraction (XRD) results suggest the formation of a uniform and compact $CH_3NH_3PbI_{3-x}Cl_x$ perovskite layer on the PCBM-modified TiO_2 blocking layer. The solar cell has reached a PCE up to 16.37%, which is greatly larger than the control device with a PCE of 10.81%.

1. Introduction

Solar cells as an economic approach to utilize solar energy have been developed for over six decades, and the most pivotal part of a solar cell is the absorber [1–6]. Recently, one material named organometal halide perovskite has caught tremendous attention in solar cell society [7–10]. Solar cells employing this kind of material have reached stunning power conversion efficiencies (PCE) of over 20% in only 6 years [11]. The organometal halide perovskite in the form of ABX_3 ($A = CH_3NH_3^+$; $B = Pb^{2+}$ or Sn^{2+}; and $X = Cl^-$, Br^-, or I^-) is a kind of promising material to absorb sunlight owning to its suitable band structure and convenient deposition process. For example, a 1.55 eV direct bandgap of $CH_3NH_3PbI_3$ is approaching the optimal bandgap for a single junction solar cell under the prediction of Shockley–Queisser limit [12]. Moreover, the solution process of organometal halide perovskite enables the use of large-scale low-cost deposition method which will further lower the cost of organometal halide perovskite solar cells [13–15].

Due to the obvious advantages, great research interests have been attracted in organometal halide perovskite solar cells in recent years [16–21]. For the record efficiency of perovskite solar cells, a mesoporous n-i-p structure was employed where n, i, and p indicate the majority carrier type in each layer of a perovskite solar cell. Compared with the mesoporous structure device, a planar heterojunction solar cell may be in more favor due to its simple device structure. The mesoporous TiO_2 high temperature (>450°C) sintering process will inevitably increase the cost of perovskite solar cells. However, for a planar n-i-p-structured organometal halide perovskite solar cell, the power conversion efficiency (PCE) still lags far behind that of mesoporous solar cells even though experiment has proved that mesoporous TiO_2 is not necessary for the electron transportation [17]. Achieving a high PCE in a planar n-i-p-structured organometal halide perovskite solar cell is not only beneficial to lower the cost of organometal halide perovskite solar cell but is also beneficial for understanding the interface properties between organometal halide perovskite solar cell and hole blocking layer.

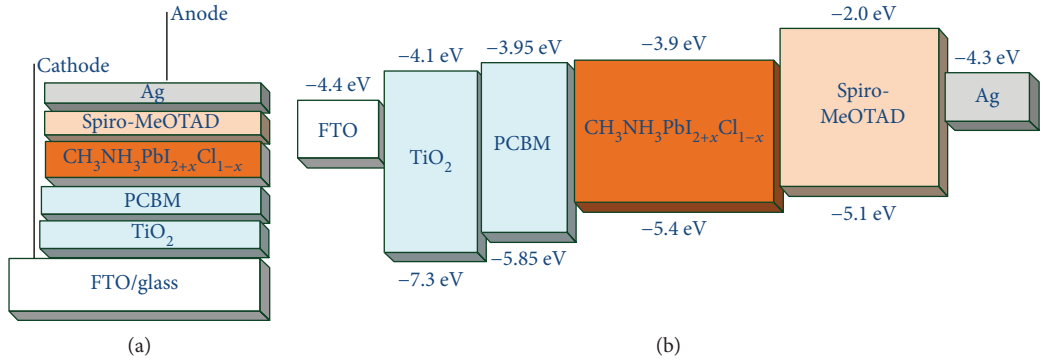

FIGURE 1: (a) The device structure of the planar heterojunction perovskite solar cell. (b) The corresponding energy level diagram. The energy levels of FTO, TiO_2, PCBM, perovskite, and spiro-MeOTAD were referenced from the previous report [22, 23].

By omitting the mesoporous TiO_2, the planar heterojunction perovskite solar cell based on the TiO_2 blocking layer has attracted much research interest. In order to achieve a better device performance, the TiO_2 blocking layer should be smooth, dense, and pinhole-free. However, when the TiO_2 is thin, pinholes usually form and when the TiO_2 is thick, a large series resistance is introduced. Both of them will decrease the device performance. Herein, we report a solution-processed TiO_2/PCBM double blocking layer to improve the device performance. It is also shown that the double blocking layer can improve the quality of $CH_3NH_3PbI_{3-x}Cl_x$ perovskite thin films. Scanning electron microscope (SEM) and atomic force microscope (AFM) photographs suggest that a dense and uniform TiO_2/PCBM blocking layer is obtained. X-ray diffraction (XRD) spectra suggest that the introduction of the PCBM layer and the following annealing process does not influence the underlying TiO_2. The as-fabricated planar heterojunction organometal halide perovskite solar cell has achieved a PCE of 16.37% with a V_{OC} of 1.05 V, a J_{SC} of 21.96 mA/cm^2, and a FF of 0.71, which is greatly larger than the control device with a PCE of 10.81%.

2. Materials and Methods

2.1. Materials. If not otherwise stated, all the materials are used as received. The materials include MAI (99.8%, Dyesol), FK-102 Cobalt salt (99.8%, Dyesol), PbI_2 (99.999%, ultra dry, Alfa), $PbCl_2$ (99.999%, Sigma-Aldrich), dimethyl sulphoxide (99.8%, anhydrous, Sigma-Aldrich), chlorobenzene (99.8%, anhydrous, Sigma-Aldrich), Li-TFSI (99.8%, Sigma-Aldrich), Toluene (99.8%, anhydrous, Sigma-Aldrich), γ-butyrolactone (99.8%, anhydrous, Aladdin), titanium diisopropoxide bis(acetylacetonate) (75 wt. % in isopropanol, Sigma-Aldrich), and 1-butanol (99.8%,Sigma-Aldrich).

2.2. Device Fabrication. Fluorine doped tin oxide (FTO, Zhuhai Kaivo Optoelectronic Technology Co. Ltd., 14 ohm/sq) glass was cleaned via sequentially in 5% Decon-90 solution, deionized water, acetone, and ethanol under ultrasonication for 15 min, respectively, and then treated with O_2 plasma for 15 min. A compact TiO_2 layer on the FTO glass was prepared by spin coating a 0.15 M titanium diisopropoxide bis(acetylacetonate) solution in 1-butanol at 2000, 4000, and 6000 rpm for 30 s, respectively, dried at 125°C for 5 min, and then repeated twice with 0.3 M of titanium diisopropoxide bis(acetylacetonate) solution, and finally, the as-prepared thin film was sintered at 500°C for 15 min. After that, the resultant TiO_2 film was immersed into a 40 mM $TiCl_4$ aqueous solution at 70°C for 30 min, washed with deionized water, and then heated at 500°C for 15 min. A 10 mg/mL PCBM solution in chlorobenzene was spin coated onto the TiO_2 film at 2000, 4000, and 6000 rpm for 45 s, respectively, and the resulted thin films were annealed at 100°C for 5 min. A $CH_3NH_3PbI_{3-x}Cl_x$ perovskite photoactive layer was deposited by dynamically spin coating a solution containing 0.14 M (39 mg) $PbCl_2$, 1.26 M (581 mg) PbI_2, and 1.3 M (209 mg) MAI in 1 mL cosolvent of DMSO:GBL (3 : 7 vol. ratio). It should be noted that the dynamically spin coating is used here so that the underlying PCBM can be avoided to be damaged when the perovskite precursor is deposited. The perovskite precursor solution was preheated at 80°C before spin coating. The spin coating was programmed to run at 1000 rpm for 40 s and then 4000 rpm for 60 s. At 20 s after the start of spin coating process, 240 μL hot $CH_3NH_3PbI_{3-x}Cl_x$ solutions was injected onto the TiO_2/PCBM blocking layer; at 60 s after the start of spin coating process, 500 μL anhydrous toluene was injected onto the spinning film to quench it. The transparent as-cast films were subsequently annealed at 100°C for 12 min. Then a spiro-MeOTAD solution containing 90 mg spiro-MeOTAD, 1 mL chlorobenzene, 45 μL LiTFSI/acetonitrile (170 mg/mL) solution, 75 μL tris (2-(1H-pyrazol-1-yl)-4-tertbutylpyridine) cobalt(III) bis(trifluoromethylsulphonyl) imide acetonitrile solution (100 mg/mL), and 10 μL tBP was spin coated on the substrates. Finally, a 100 nm Ag film was thermally evaporated as the anode.

2.3. Measurements. The morphology measurement of the perovskite layers were measured by SEM (Quanta x50 FEG) and AFM (Bruker Dimension Icon). XRD test was conducted on Bruker D8 advanced, and the samples were prepared as the same process of device fabrication. The UV-visible absorption spectra of TiO_2, TiO_2/PCBM, and

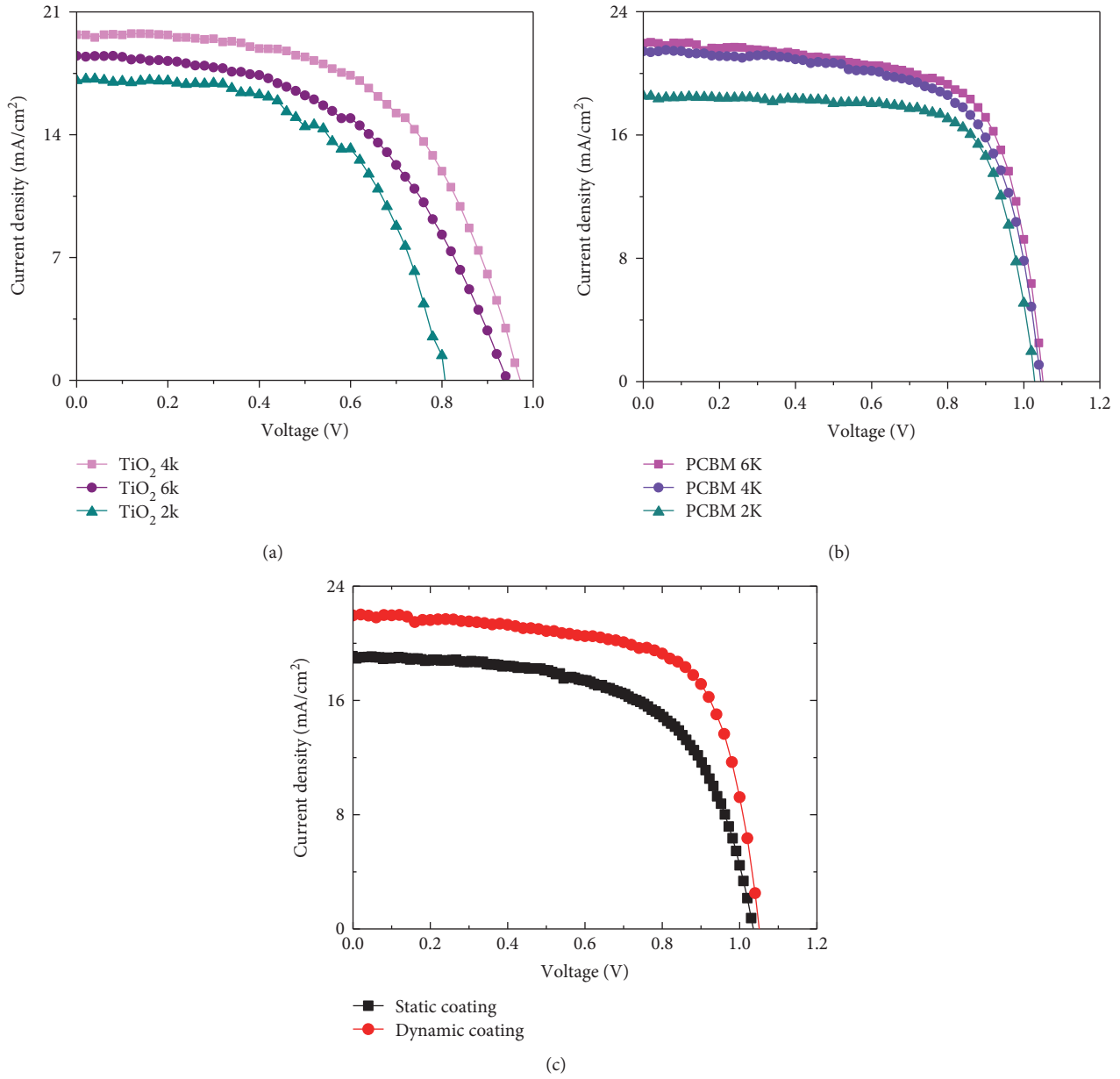

Figure 2: (a) Photovoltaic performance of perovskite solar cells prepared at different TiO_2 spin coating speed. (b) Photovoltaic performance of perovskite solar cells prepared at different PCBM spin coating speed (the TiO_2 spin coating speed was fixed at 4000 rpm). (c) The device performance fabricated by the static coating method and the dynamic coating method. The TiO_2 spin coating speed was fixed at 4000 rpm, and the PCBM spin coating speed was fixed at 6000 rpm.

Table 1: Photovoltaic performance of different blocking layer.

Blocking layer	J_{SC} (mA/cm^2)	V_{OC} (V)	FF	PCE (%)
TiO_2 2k	17.09	0.81	0.57	7.90
TiO_2 4k	19.70	0.98	0.56	10.81
TiO_2 6k	18.49	0.94	0.52	9.03
TiO_2 4k PCBM 2k	18.54	1.02	0.71	13.42
TiO_2 4k PCBM 4k	21.42	1.05	0.67	15.06
TiO_2 4k PCBM 6k	21.96	1.05	0.71	16.37

Table 2: Photovoltaic performance of different coating methods.

Coating method	J_{SC} (mA/cm^2)	V_{OC} (V)	FF	PCE (%)
Static coating	19.10	1.04	0.62	12.3
Dynamic coating	21.96	1.05	0.71	16.37

$CH_3NH_3PbI_{3-x}Cl_x$ were recorded with UV-visible spectrophotometer (Perkin-Elmer Lambda 950) using the precleaned FTO glass as the blank signal. Photovoltaic performances were measured by using Keithley 2400 source meter under simulated sunlight from XES-70S1 solar simulator matching the AM 1.5G standard. The system was calibrated against a NREL-certified reference solar cell. All the measurements of the solar cells were

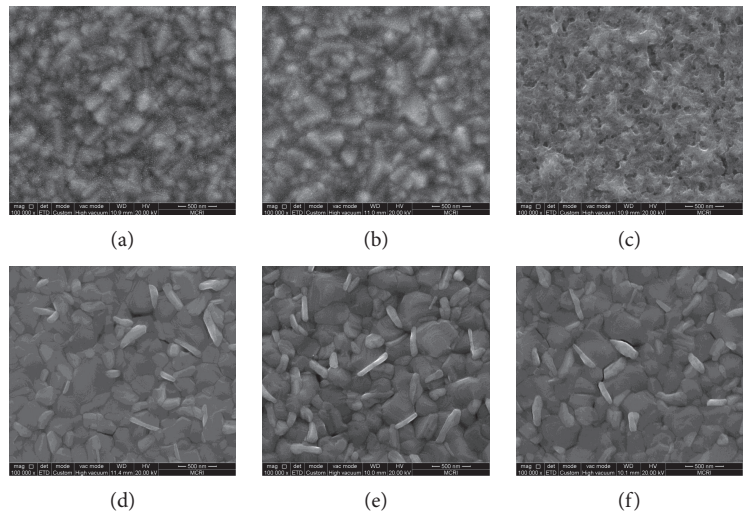

Figure 3: SEM photographs of TiO_2 thin films prepared at (a) 2000 rpm, (b) 4000 rpm, and (c) 6000 rpm, respectively. And SEM photographs of $CH_3NH_3PbI_{3-x}Cl_x$ on TiO_2/PCBM thin films, with TiO2 prepared at 4000 rpm and PCBM at (d) 2000 rpm, (e) 4000 rpm, and (f) 6000 rpm.

performed with the active area of 0.07 cm^2 under ambient atmosphere at room temperature without encapsulation.

3. Results and Discussion

The planar heterojunction perovskite solar cell in this study is structured as FTO/TiO_2 (with or without PCBM)/$CH_3NH_3PbI_{3-x}Cl_x$/spiro-MeOTAD/Ag as shown in Figure 1, where the TiO_2 and spiro-MeOTAD act as hole and electron blocking layers, respectively. Figure 2(a) shows the photocurrent-voltage (J-V) curves of TiO_2 hole blocking layer with different spin coating speed. Table 1 summarizes the device performance of these perovskite solar cells. When the TiO_2 spin coating speed is 2000 rpm, the device achieves a PCE of 7.90% with J_{SC} of 17.09 mA/cm^2, V_{OC} of 0.81 V, and FF of 0.57. In increasing the spin coating speed from 2000 rpm to 4000 rpm, the PCE increases from 7.90 to 10.81%. However, when the spin coating speed of TiO_2 is further increased to 6000 rpm, a decrease in PCE along and a poor reproductivity are observed.

By increasing the spin coating speed of TiO_2 from 2000 rpm to 4000 rpm, the V_{OC} increased from 0.81 V to 0.98 V with the J_{SC} increased from 17.09 mA/cm^2 to 19.07 mA/cm^2 and the fill factor does not change much. This indicates that a thicker TiO_2 blocking layer caused a large series resistance and this series resistance leads to the V_{OC} and J_{SC} losses. While further increasing the spin coating speed does not improve the device performance, at a TiO_2 spin coating speed of 6000 rpm, the corresponding devices show a lower FF which may correspond to the increase of current leakage. It is worth to notice that optimizing the spin coating speed of TiO_2 does not yield a FF over 70% which can be easily obtained in a mesoporous n-i-p-structured perovskite solar cell. Here, PCBM is introduced to modify the TiO_2 layer and PCBM in this structure is expected to perform threefold functions: firstly, PCBM can reduce the energy mismatch between TiO_2 and the perovskite film and facilitate the electron transport from the perovskite film to the TiO_2 layer; secondly, PCBM can improve the compactness of the electron transporting layer and avoid the direct contact between perovskite film and the FTO electrode; thirdly, PCBM is expected to have a passivation effect in the devices, which has been proved by recent studies [19, 20]. The photocurrent-voltage (J-V) curves with PCBM-modified TiO_2 layer are shown in Figure 2(b).

From Figure 2(b), it could be seen that the insertion of PCBM is mainly in favor of the increase of FF and V_{OC}. As it is known, the V_{OC} of a solar cell corresponds to the splitting of quasi-fermi level and the insertion of PCBM could reduce the trap state density which can further increase the splitting [20]. Hence compared with TiO_2 only device, PCBM-modified device has reached a V_{OC} of 1.05 V and the FF enhancement may owe the suitable band structure of PCBM which may reduce the energy offset between perovskite and TiO_2. With the help of PCBM layer, the device achieved a PCE of 16.37% with a J_{SC} of 21.96 mA/cm^2, V_{OC} of 1.05 V, and FF of 0.71 when the PCBM spin coating speed is 6000 rpm. When the PCBM layer is thick, the series resistance is large. Then with the increasing PCBM spin coating speed, the device PCE is improved. However, a too high PCBM spin coating speed will make it difficult to form a continuous and full coverage PCBM layer as shown in the formation of TiO_2 layer. In fact, a PCBM spin coating speed more than 6000 rpm will lead to the decreased device performance and the 6000 rpm for PCBM solution is optimal.

It should be noted that all the devices above are fabricated by the dynamic coating method when depositing the perovskite precursor on top of the underlying PCBM layer. It was found that the coating method could greatly affect the final device performance. Figure 1 shows the performance difference between the two devices fabricated by the different coating methods. For both the devices, the PCBM layer is formed by spin coating a 10 mg/mL PCBM solution in chlorobenzene onto the TiO_2 film at 6000 rpm for 45 s. The

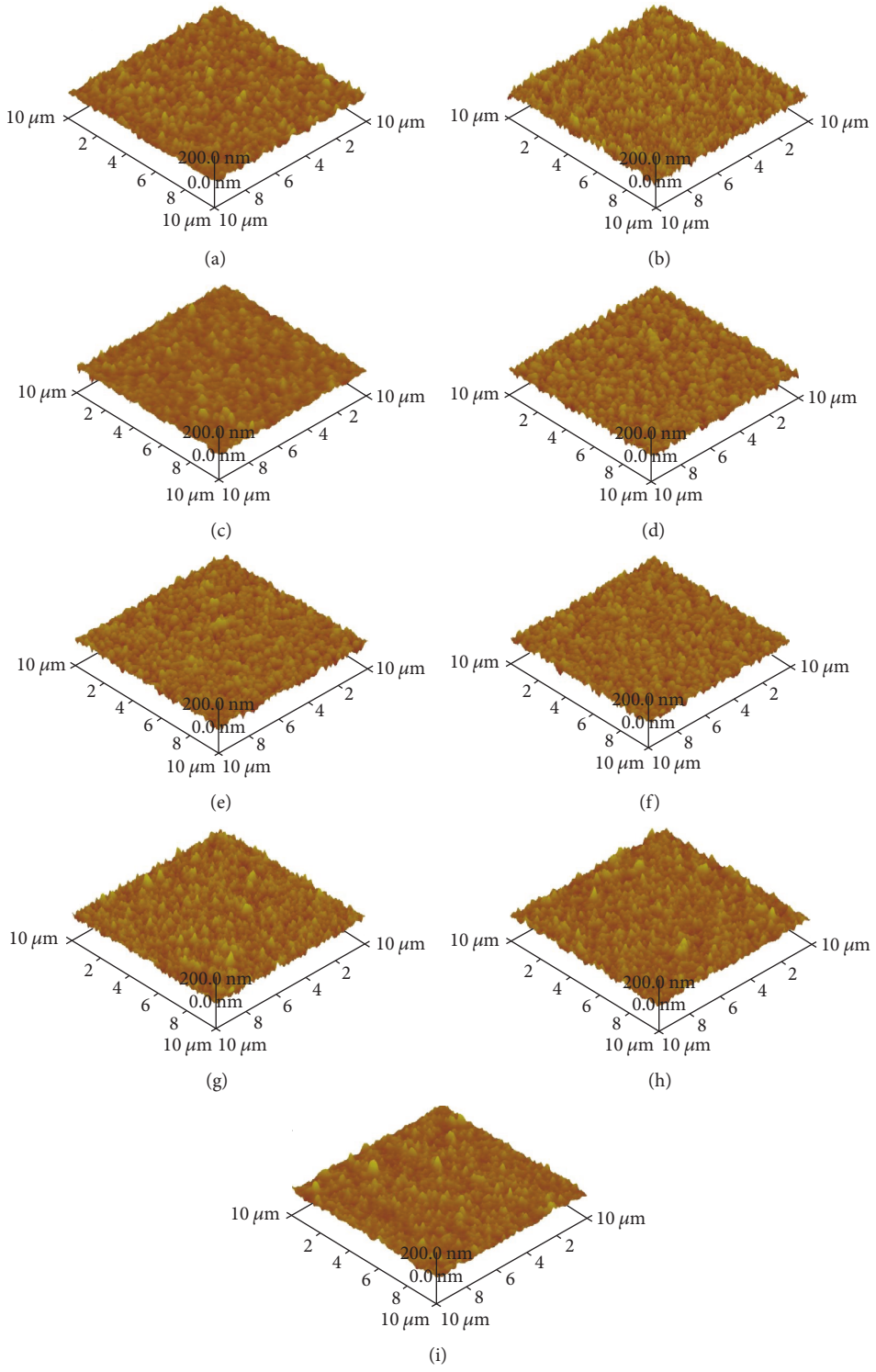

FIGURE 4: AFM photographs of TiO_2 thin films prepared at (a) 2000 rpm, (b) 4000 rpm, and (c) 6000 rpm, respectively. The root mean square roughness (RMS) value of TiO_2 thin films prepared at 2000, 4000, and 6000 rpm was 10.4 nm, 13.2 nm, and 18.4 nm, respectively. AFM photograph of TiO2/PCBM thin films with TiO_2 prepared at 4000 rpm and PCBM at (d) 2000 rpm, (e) 4000 rpm, and (f) 6000 rpm, respectively. RMS roughness for (d) is 15.6 nm, (e) is 15.3 nm, and (f) is 16.0 nm. AFM photographs of $CH_3NH_3PbI_{3-x}Cl_x$ organometal halide perovskite material, with a constant spin coating speed of TiO_2 at 4000 rpm and PCBM at (g) 2000 rpm, (h) 4000 rpm, and (i) 6000 rpm, respectively. RMS roughness for (g) is 15.6 nm, (h) is 13.8 nm, and (i) is 12.2 nm.

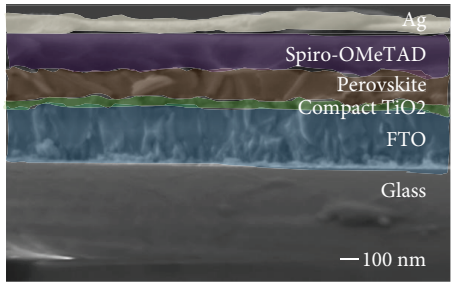

Figure 5: Cross-section image of the complete device with the structure of FTO/TiO_2/PCBM/$CH_3NH_3PbI_{3-x}Cl_x$/spiro-OMeTAD/Ag. The TiO_2 spin coating speed was fixed at 4000 rpm, and the PCBM spin coating speed was fixed at 6000 rpm. Because the PCBM layer is thin, the separate TiO_2 layer and the PCBM layer cannot be distinguished. This TiO_2/PCBM bilayer is denoted as compact TiO_2 in this image.

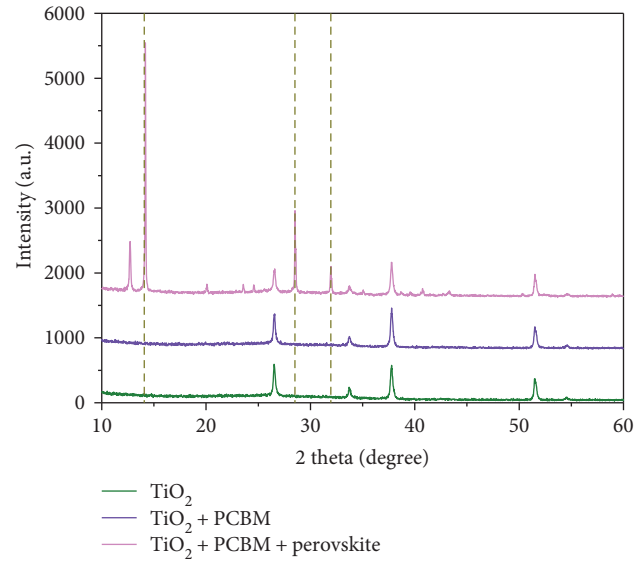

Figure 6: XRD spectra of TiO_2, TiO_2/PCBM, and $CH_3NH_3PbI_{3-x}Cl_x$.

difference between them is that one device is fabricated by coating the following perovskite precursor with the dynamic method (labeled as "dynamic coating") and another one is fabricated by coating the following perovskite precursor with the static method (labeled as "static coating"). The corresponding device parameters are summarized in Table 2. For the device with the static coating method, it achieved a PCE of 12.3% with a J_{SC} of 19.10 mA/cm^2, V_{OC} of 1.04 V, and FF of 0.62, which is greatly inferior to the device with the dynamic coating method. It could be clearly obtained that the dynamic coating method could greatly improve the device performance. We believe that the reason is that the dynamically spin coating could avoid the serious damage of the underlying PCBM when the perovskite precursor is deposited. The PCBM layer plays an important role to improve the device performance. Xing et al. [24] showed that there are high density hole-deficient traps located at the TiO_2 surface, which leads to an electron transfer potential barrier between $CH_3NH_3PbI_3$ and TiO_2. This potential barrier is absent between the perovskite layer and the PCBM layer, and then the PCBM layer has a faster charge extraction compared to TiO_2 [24, 25]. In order to ensure the function of PCBM, the PCBM layer should be avoided from the damage when the perovskite precursor is deposited. This is why the device with the dynamic coating method has a better device performance.

In order to achieve a good performance, the TiO_2 layer in the planar heterojunction perovskite solar cell should be compact and pinhole-free. If there are pinholes in the TiO_2 layer, it is possible that the perovskite film can direct contact with the FTO electrode, which will lead to severe recombination at the FTO and perovskite film interface and result in a low short-circuit current density (J_{SC}) and a low open-circuit voltage (V_{OC}). It is possible to achieve a pinhole-free TiO_2 layer by increasing the TiO_2 film thickness. However, a too thick TiO_2 blocking layer corresponds to a large series resistance and low fill factor as shown in the previous work [22]. To investigate the influence of spin coating speed on the morphology of TiO_2 thin film, SEM photographs were taken on TiO_2 thin films prepared at 2000, 4000, and 6000 rpm, corresponding to Figures 3(a)–3(c), respectively (the SEM photographs in large scale in Supplementary Figure S1). Pinholes are observed on the TiO_2 thin film which is prepared at a spin coating speed of 6000 rpm. And no pinholes are found on TiO_2 thin films at the spin coating speed of 2000 and 4000 rpm.

Figures 4(a)–4(c) show the corresponding AFM images. The root mean square roughness (RMS) value of TiO_2 thin films prepared at 2000, 4000, and 6000 rpm is 10.4 nm, 13.2 nm, and 18.4 nm, respectively. It could be seen that the film roughness is improved with the increase of the spin coating speed. When there are no pinholes, the roughness increasing is small. However, when the pinholes appear, the roughness increasing is severe. Thus, when the TiO_2 thin film is prepared at a spin coating speed of 4000 rpm, the film is pinhole-free and at the same time, the thickness is low and relative smooth. This TiO_2 thin film would be used for the following discussion.

By introducing PCBM into the blocking layer, the blocking layer is improved which will be in favor for the electron extraction as the electrical measurements shown in Figure 2(b). Figure 4 and Supplementary Figure S1 present the AFM and SEM photographs of PCBM/TiO_2 blocking layer, the spin coating speed of TiO_2 is fixed to 4000 rpm, and the spin coating speed of PCBM varied from 2000 rpm to 6000 rpm at a 2000 interval. As the Supplementary Figure S1 (d), (e), and (f) depicted, when PCBM was introduced, no pinholes are observed, and the spin coating speed could hardly affect the morphology of TiO_2/PCBM thin films. As shown in the AFM photographs, the roughness of TiO_2/PCBM thin films could be deduced. As Figures 4(d)–4(f) illustrated, the RMS value of TiO_2/PCBM thin films prepared at 2000, 4000, and 6000 rpm is almost the same and in the range from 15 nm to 16 nm. By increasing the spin coating speed, negligible variances in RMS values

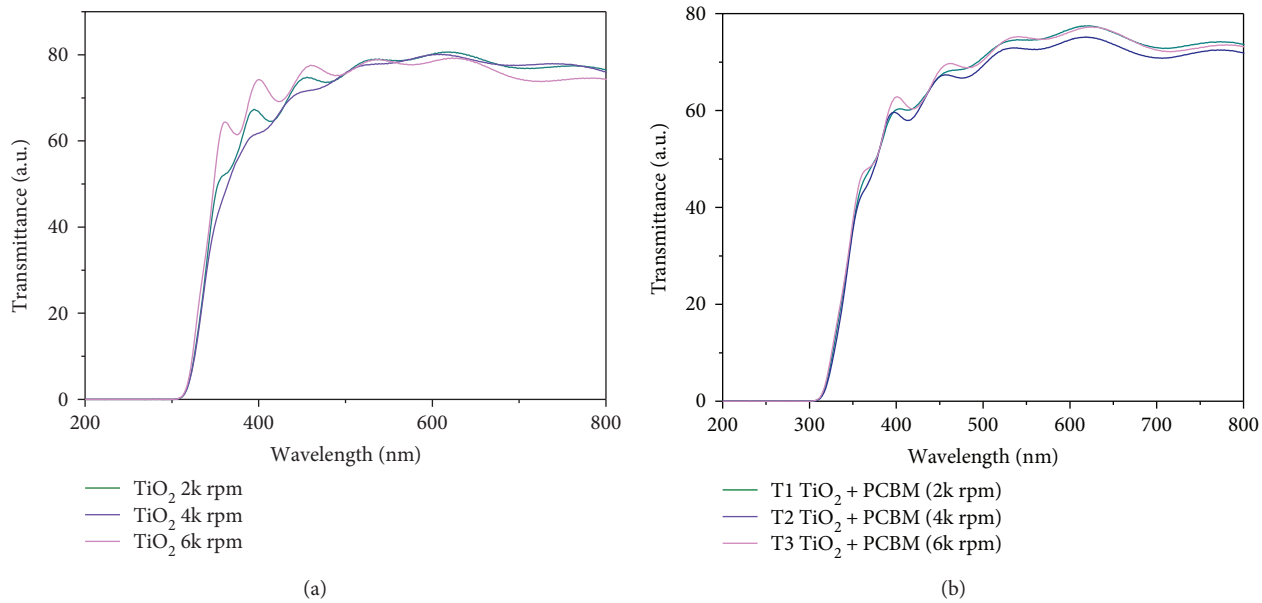

FIGURE 7: (a) UV-vis spectra of TiO_2 thin films with spin coating speed at 2000, 4000, and 6000 rpm, respectively. (b) UV-vis spectra of TiO_2/PCBM thin films with spin coating speed at 2000, 4000, and 6000 rpm, respectively.

are observed. It is shown that the RMS values are mainly determined by the underlying TiO_2 layer.

To further investigate the morphology of $CH_3NH_3PbI_{3-x}Cl_x$ organometal halide perovskite material deposited on TiO_2/PCBM thin films, SEM and AFM photographs of $CH_3NH_3PbI_{3-x}Cl_x$ are taken on TiO_2/PCBM thin films, with TiO_2 spin coating speed fixed at 4000 rpm and the PCBM spin coating speed varied from 2000 rpm to 6000 rpm at a 2000 interval. It could be found that dense and uniform $CH_3NH_3PbI_{3-x}Cl_x$ organometal halide perovskite thin film is obtained on the TiO_2/PCBM thin film. SEM photographs in Figures 3(d)–3(f) (the SEM photographs in large scale in Supplementary Figure S1) suggest that the grain sizes of the $CH_3NH_3PbI_{3-x}Cl_x$ film are in a range of 450–550 nm, which is almost double the size of $CH_3NH_3PbI_{3-x}Cl_x$ directly on the TiO_2 layer as shown in our previous work [22]. This is because that the PCBM layer is more hydrophobic than the TiO_2 layer, and a hydrophobic PCBM layer can help increase the perovskite crystal size [26]. This grain size value is slightly larger than the film thickness (about 300 nm from the XRD measurement and also could be seen from the Figure 5), which implies that it is great possible that the carrier could pass the perovskite film without encountering any grain boundaries. The granular particle between $CH_3NH_3PbI_{3-x}Cl_x$ grain boundaries is PbI_2 as in the previous report [19], which might passivate $CH_3NH_3PbI_{3-x}Cl_x$ material. This result also coincidences with our following XRD analysis. Figures 4(g)–4(i) show the AFM photographs of $CH_3NH_3PbI_{3-x}Cl_x$ organometal halide perovskite materials. With a constant spin coating speed of TiO_2 at 4000 rpm, the spin coating speed and RMS roughness of PCBM are (Figure 4(g)) 2000 rpm with a 15.6 nm RMS roughness, (Figure 4(h)) 4000 rpm with a 13.8 nm RMS roughness, and (Figure 4(i)) 6000 rpm with a 12.2 nm RMS roughness. It suggests that increasing the spin coating speed results in a decrease of RMS roughness.

After the above discussion on morphology, X-ray diffraction measurement is carried out to investigate the crystallization of the thin films. As shown in Figure 6, the peaks at 37.74° and 51.50° belongs to FTO and the peaks at 26.52° and 36.71° belongs to TiO_2 suggesting an anatase crystal structure. As shown in Supplementary Figure S2, the TiO_2 films prepared at 2000 rpm, 4000 rpm, and 6000 rpm show the similar XRD spectra and this means that the spin coating speed does not change the underlying layer. By analyzing the XRD spectra of TiO_2 and TiO_2/PCBM thin films, it is found that the introduction of PCBM at various spin coating speeds and the consequence annealing process does not influence the crystallization of TiO_2 and $CH_3NH_3PbI_{3-x}Cl_x$ as shown in Figure 6 and Supplementary Figure S3. For the TiO_2/PCBM/$CH_3NH_3PbI_{3-x}Cl_x$ XRD spectra, the weak peak at 12.72° corresponds to PbI_2 and this coincides with the SEM photograph. Different from the spectra of TiO_2 and TiO_2/PCBM thin films, three strong peaks appeared at 14.17°, 28.51°, and 31.95°, which correspond to <110>, <220>, and <310> lattice planes of the tetragonal perovskite structure, respectively.

To further illustrate the optical characteristics of TiO_2/PCBM thin films, UV-vis spectra are carried out. Figure 7(a) depicts the UV-vis spectra of TiO_2 thin films, and Figure 7(b) depicts the UV-vis spectra TiO_2/PCBM thin films. As it could be seen from Figure 7, increasing the spin coating speed of TiO_2 leads to a decrease in transmittance. On the contrary, increasing the spin coating speed of PCBM leads to an increase in transmittance. The conflict lies in the morphology and optical absorption of TiO_2 and PCBM. As AFM photographs demonstrate, when spin coated at 6000 rpm, pinholes are observed on TiO_2 surface along with

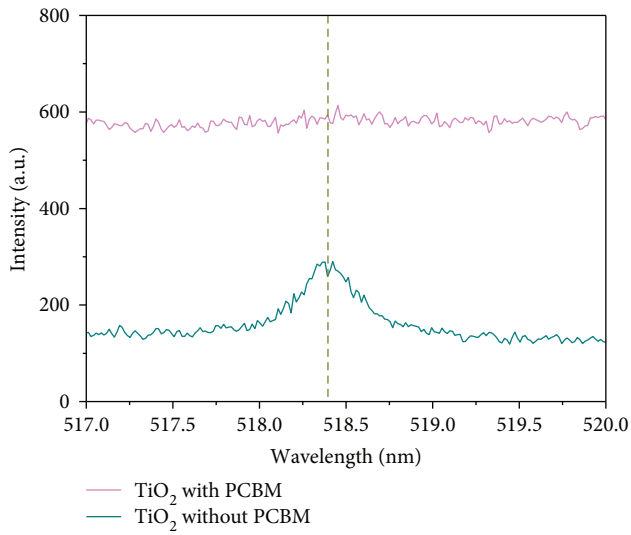

Figure 8: PL spectra of the TiO_2 films with/without the PCBM layer.

an increase in RMS roughness. In agreement with our previous report [22], this roughness causes the scattering of incident light hence leads to the decrease in transmittance. While PCBM is a commonly used material in organic solar cell, a thicker PCBM layer absorbs more incident light, which leads to the decrease in transmittance.

This decrease in PCE is attributed to the pinholes in TiO_2 prepared at 6000 rpm spin coating speed that has been supported by the SEM photograph. In Figure S4, PL spectra of TiO_2 thin film have suggested a peak at 518.4 nm corresponding to the thickness of TiO_2 thin film. Since our exciton wavelength is 515 nm, which could not satisfy the excitation requirement of bulk TiO_2, the peak corresponds to the surface trap of TiO_2 thin film which may greatly influence the photovoltaic performance of solar cells [27, 28]. After spin coated a thin PCBM layer as shown in Figure 8, the PL peak at 518.4 nm could hardly be observed, which further proves the suggestion that the peak corresponds to the surface trap of TiO_2 thin film and the PCBM could passivate the traps.

4. Conclusions

Herein, a versatile TiO_2/PCBM double blocking layer was introduced into the planar heterojunction perovskite solar cell. The PCBM layer has faster charge extraction compared to TiO_2. At the same time, by employing PCBM, the TiO_2 thin film was efficiently passivated and the hydrophobic PCBM also yields a large grain size pinhole-free $CH_3NH_3PbI_{3-x}Cl_x$ thin film. Utilizing the as-prepared thin film, the planar heterojunction organometal halide perovskite solar cell has shown improved performance compared to the control device, achieving a PCE of 16.37%, a V_{OC} of 1.05 V, a J_{SC} of 21.96 mA/cm^2, and an FF of 0.71.

Conflicts of Interest

The authors declare that there is no conflict of interest regarding the publication of this paper.

Acknowledgments

This study was partly financially supported by the National Natural Science Foundation of China (61334002, 61106063, and 61534004) and the Fundamental Research Funds for the Central Universities (JB141106).

Supplementary Materials

Supplementary 1. Figure S1: SEM photographs of TiO_2 thin films prepared at (a) 2000 rpm, (b) 4000 rpm, and (c) 6000 rpm, respectively. SEM photographs of TiO_2/PCBM thin films with TiO_2 prepared at 4000 rpm and PCBM prepared at (d) 2000 rpm, (e) 4000 rpm, and (f) 6000 rpm, respectively. And SEM photographs of $CH_3NH_3PbI_{3-x}Cl_x$ on TiO_2/PCBM thin films, the PCBM spin-coating speed is (g) 2000 rpm, (h) 4000 rpm, and (i) 6000 rpm.
Supplementary 2. Figure S2: XRD spectra of TiO_2 thin films prepared at (a) 2000 rpm, (b) 4000 rpm, and (c) 6000 rpm, respectively.
Supplementary 3. Figure S3: XRD spectra of TiO_2 thin films prepared at (a) 2000 rpm, (b) 4000 rpm, and (c) 6000 rpm, respectively.
Supplementary 4. Figure S4: XRD spectra of TiO_2 thin films prepared at (a) 2000 rpm, (b) 4000 rpm, and (c) 6000 rpm, respectively.

References

[1] C. C. Chen, W. H. Chang, K. Yoshimura et al., "An efficient triple-junction polymer solar cell having a power conversion efficiency exceeding 11%," *Advanced Materials*, vol. 26, no. 32, pp. 5670–5677, 2014.

[2] L. P. Heiniger, F. Giordano, T. Moehl, and M. Grätzel, "Mesoporous TiO_2 beads offer improved mass transport for cobalt-based redox couples leading to high efficiency dye sensitized solar cells," *Advanced Energy Materials*, vol. 4, no. 12, article 1400168, 2014.

[3] Y. He, Y. Lei, X. Yang et al., "Using elemental Pb surface as a precursor to fabricate large area $CH_3NH_3PbI_3$ perovskite solar cells," *Applied Surface Science*, vol. 389, pp. 540–546, 2016.

[4] Y.-Y. Lee, W.-J. Ho, and C.-W. Yeh, "Fabrication of silicon solar cell with >18% efficiency using spin-on-film processing for phosphorus diffusion and SiO2/graded index TiO_2 anti-reflective coating," *Applied Surface Science*, vol. 354, pp. 20–24, 2015.

[5] D. Chen, C. Zhang, T. Heng et al., "Efficient inverted polymer solar cells using low-temperature zinc oxide interlayer processed from aqueous solution," *Japanese Journal of Applied Physics*, vol. 54, no. 4, article 042301, 2015.

[6] Z. Wang, C. Zhang, R. Gao et al., "Improvement of transparent silver thin film anodes for organic solar cells with a decreased percolation threshold of silver," *Solar Energy Materials & Solar Cells*, vol. 127, pp. 193–200, 2014.

[7] Z. Xiao, Y. Yuan, Y. Shao et al., "Giant switchable photovoltaic effect in organometal trihalide perovskite devices," *Nature Materials*, vol. 14, no. 2, pp. 193–198, 2015.

[8] D. P. McMeekin, G. Sadoughi, W. Rehman et al., "A mixed-cation lead mixed-halide perovskite absorber for tandem solar cells," *Science*, vol. 351, no. 6269, pp. 151–155, 2016.

[9] N. Ahn, D. Y. Son, I. H. Jang, S. M. Kang, M. Choi, and N. G. Park, "Highly reproducible perovskite solar cells with average efficiency of 18.3% and best efficiency of 19.7% fabricated via Lewis base adduct of lead (II) iodide," *Journal of the American Chemical Society*, vol. 137, no. 27, pp. 8696–8699, 2015.

[10] N. J. Jeon, J. H. Noh, Y. C. Kim, W. S. Yang, S. Ryu, and S. I. Seok, "Solvent engineering for high-performance inorganic–organic hybrid perovskite solar cells," *Nature Materials*, vol. 13, no. 9, pp. 897–903, 2014.

[11] W. S. Yang, J. H. Noh, N. J. Jeon et al., "High-performance photovoltaic perovskite layers fabricated through intramolecular exchange," *Science*, vol. 348, no. 6240, pp. 1234–1237, 2015.

[12] W. Shockley and H. J. Queisser, "Detailed balance limit of efficiency of p-n junction solar cells," *Journal of Applied Physics*, vol. 32, no. 3, pp. 510–519, 1961.

[13] W. Chen, Y. Wu, Y. Yue et al., "Efficient and stable large-area perovskite solar cells with inorganic charge extraction layers," *Science*, vol. 350, no. 6263, pp. 944–948, 2015.

[14] K. Hwang, Y. S. Jung, Y. J. Heo et al., "Toward large scale roll-to-roll production of fully printed perovskite solar cells," *Advanced Materials*, vol. 27, no. 7, pp. 1241–1247, 2015.

[15] Y. Deng, E. Peng, Y. Shao, Z. Xiao, Q. Dong, and J. Huang, "Scalable fabrication of efficient organolead trihalide perovskite solar cells with doctor-bladed active layers," *Energy & Environmental Science*, vol. 8, no. 5, pp. 1544–1550, 2015.

[16] G. Xing, N. Mathews, S. Sun et al., "Long-range balanced electron-and hole-transport lengths in organic-inorganic $CH_3NH_3PbI_3$," *Science*, vol. 342, no. 6156, pp. 344–347, 2013.

[17] S. D. Stranks, G. E. Eperon, G. Grancini et al., "Electron-hole diffusion lengths exceeding 1 micrometer in an organometal trihalide perovskite absorber," *Science*, vol. 342, no. 6156, pp. 341–344, 2013.

[18] M. Liu, M. B. Johnston, and H. J. Snaith, "Efficient planar heterojunction perovskite solar cells by vapour deposition," *Nature*, vol. 501, no. 7467, pp. 395–398, 2013.

[19] Y. Shao, Z. Xiao, C. Bi, Y. Yuan, and J. Huang, "Origin and elimination of photocurrent hysteresis by fullerene passivation in $CH_3NH_3PbI_3$ planar heterojunction solar cells," *Nature Communications*, vol. 5, p. 5784, 2014.

[20] Y. Shao, Y. Yuan, and J. Huang, "Correlation of energy disorder and open-circuit voltage in hybrid perovskite solar cells," *Nature Energy*, vol. 1, no. 1, article 15001, 2016.

[21] C. Tao, S. Neutzner, L. Colella et al., "17.6% stabilized efficiency in low-temperature processed planar perovskite solar cells, energy," *Environmental Sciences*, vol. 8, pp. 2365–2370, 2015.

[22] C. Zhang, S. Tang, J. Yan et al., "Efficient planar heterojunction solar cell employing $CH_3NH_3PbI_{2+x}Cl_{1-x}$ mixed halide perovskite utilizing modified sequential deposition," *Japanese Journal of Applied Physics*, vol. 54, no. 9, article 092301, 2015.

[23] P. Docampo, J. M. Ball, M. Darwich, G. E. Eperon, and H. J. Snaith, "Efficient organometal trihalide perovskite planar-heterojunction solar cells on flexible polymer substrates," *Nature Communications*, vol. 4, p. 2761, 2013.

[24] G. Xing, B. Wu, S. Chen et al., "Interfacial electron transfer barrier at compact $TiO_2/CH_3NH_3PbI_3$ heterojunction," *Small*, vol. 11, no. 29, pp. 3606–3613, 2015.

[25] L. Kegelmann, C. M. Wolff, C. A. Omondi et al., "It takes two to tango—double-layer selective contacts in perovskitesolar cells for improved device performance and reduced hysteresis," *ACS Applied Materials & Interfaces*, vol. 9, no. 20, pp. 17245–17255, 2017.

[26] C. Bi, Q. Wang, Y. Shao, Y. Yuan, Z. Xiao, and H. Huang, "Non-wetting surface-driven high-aspect-ratio crystalline grain growth for efficient hybrid perovskite solar cells," *Nature Communications*, vol. 6, p. 7747, 2015.

[27] Y. Lei, L. D. Zhang, G. W. Meng et al., "Preparation and photoluminescence of highly ordered TiO_2 nanowire arrays," *Applied Physics Letters*, vol. 78, no. 8, pp. 1125–1127, 2001.

[28] X. Wang, Z. Feng, J. Shi et al., "Trap states and carrier dynamics of TiO_2 studied by photoluminescence spectroscopy under weak excitation condition," *Physical Chemistry Chemical Physics*, vol. 12, no. 26, pp. 7083–7090, 2010.